Research on Underwater Acoustic Target Depth Classification Based on Modal Filtering Characteristics of Long Horizontal Line Array

Guojun Xu, Weihua Zhang, Min Zhu, Jizhou Guo, Yanqun Wu and Jiahua Zhu
National University of Defense Technology, Changsha, 410073, China. E-mail: xuguojun@nudt.edu.cn

(Received 29 July 2021; accepted 4 January 2022)

Considering the problem of depth classification of underwater acoustic targets in shallow water, a classification method based on modal filtering characteristics of long horizontal line array(HLA) beamforming in anegative thermocline environment was proposed. Based on normal mode theory, the spatial filtering characteristics of long HLA are studied by beamforming, and it was found that this characteristic can filter a normal mode. In the negative thermocline environment, the acoustic fields excited by deep and shallow sources and received by deep receivers are controlled by different modes. Surface reflection bottom reflection (SRBR) mode and non-surface reflection bottom reflection (NSRBR) mode show different interference structures in range-spectrum. Based on the characteristics of modal filtering and sound field classification, a depth classification method for shallow water acoustic targets in negative thermocline environment is established. Numerical results show that the proposed method is robust and can effectively distinguish the acoustic source targets above or below the thermocline (surface and underwater targets) without knowing the specific acoustic environment parameters in advance.

1. INTRODUCTION

The discrimination of surface and underwater targets has always been an important scientific problem in the field of underwater acoustic engineering, which plays an important role in improving the performance of underwater acoustic equipment. The commonly used surface and underwater target identification methods mainly rely on the underwater acoustic channel characteristics or the target noise characteristics. Among them, the main methods of using channel characteristics are matched field processing,[1,2] array-based sound field analysis[3–5] etc. However, this kind of method has some disadvantages, such as high requirements of underwater acoustic environment parameters, complex arrangement of acoustic information acquisition equipment, etc. The main methods of using target noise features are based on machine learning image processing,[6] target radiated noise feature analysis,[7,8] and deep learning.[9,10] These kinds of method obtain robust identification results when the target samples are sufficient. However, in practice, due to the small number of data samples of underwater targets, the accuracy of target classification estimated by this method is generally poor.

In shallow water, when the acoustic pressure is represented by the normal mode theory, it can be composed of a series of normal modes.[11] The interference structure in the range-frequency spectrum of the acoustic intensity generated by the combination of different modes (SRBR or NSRBR) will be significantly different. When the waveguide invariant is used to characterize the striations characteristics, different interference striation angles correspond to different waveguide invariant. For example, the waveguide invariant corresponding to the SRBR mode is about 1, while that corresponding to the NSRBR mode may be negative or greater than 1.

The shallow water area around China has typical negative thermocline sound velocity profile environment in the summer, and the acoustic field radiated by the target above the thermocline that is a surface target, received by a subsea fixed horizontal array is mainly composed of SRBR modes. However, the acoustic field radiated by the target under the thermocline that isan underwater target, is mainly composed of refraction bottom reflected (RBR) modes. For these two kinds of targets, there is a significant difference in the interference striations of the acoustic intensity range-frequency spectrum output from a large depth receiver, and can be used to classify the depth of the target. A technique of frequency adaptive optimal weight (FAOW) array beam processing is introduced in Ref.12. The mode's filter is realized by designing the weight of array elements in the process of beamforming, so that the acoustic field after the array beamforming is mainly composed of SRBR modes.

In shallow negative thermocline water, the radiated acoustic field from the surface acoustic target outputted by the single hydrophone or the filtered array beam are composed of SRBR modes. There is no obvious difference in the range-spectrum interference structure of the acoustic intensity. For the underwater target, the radiated acoustic field received by a single hydrophone is mainly composed of RBR modes, while the filtered array beam is mainly composed of SRBR modes, meaning that their intensity range-spectrum interference structures are obviously different. Therefore, the surface and underwater attribute classification of underwater acoustic targets can be realized by using the mode filtering characteristics of the long HLA beamforming.

In Section 2, the classification of acoustic field modes is introduced. In Section 3, the acoustic field expression of the HLA beamforming is first derived, and the filtering characteristic of long HLA beam output is analyzed according to the normal mode theory. Based on the mode's filtering characteristics of the long HLA, a depth classification method for underwater acoustic targets in a negative thermocline environment is constructed. Section 4 conducts numerical analyses of the above classification methods.

2. ACOUSTIC MODES CLASSIFICATION

When the acoustic source and receiver are separated by a distance greater than several water depths, for range independent bathymetries, the complex pressure as a function of range from the source *r*, depth *z*, and frequency ω can be written as:

$$p\left(r,z,\omega\right)=\frac{i}{\sqrt{8\pi r}\rho\left(z_s\right)}e^{-i\pi/4}\sum_{m=1}^{\infty}\varphi_m\left(z_s\right)\varphi_m\left(z\right)\frac{e^{ik_{rm}r}}{\sqrt{k_{rm}}}; \tag{1}$$

where z_s is the source depth; k_{rm} is the horizontal wavenumber of mode *m*, and $\phi_m(z)$ is the mode function of mode *m*; k_{rm} and $\phi_m(z)$ usually depend on radian frequency ω and the sound speed profile $c(z)$. The acoustic pressure field is a finite sum of normal modes.

Refs.[11] and[14] show that there are two types of modes: SRBR modes and NSRBR modes. The SRBR modes have $\omega/c_{seafloor} < k_{rm} < \omega/c_{max}$ or $c_{max} < v_{pm} < c_{seafloor}$ where c_{max} is the maximum sound speed in the water column (not including the sea floor), and $c_{seafloor}$ is the sound speed of the sea floor. The term NSRBR will be used to refer to any mode that is not an SRBR mode. NSRBR modes always have $\omega/c_{max} < k_{rm} < \omega/c_{min}$ or $c_{min} < v_{pm} < c_{max}$, where c_{min} is the minimum sound speed on the water column, and v_{pm} is the phase velocities for a mode *m*.

According to the invariant relationship of acoustic field waveguides in shallow water described in Ref.,[15] simulations have been conducted to illustrate the relationship between group velocities and phase velocities of all modes corresponding under different sound velocity profiles, as shown in Fig. 1. The waveguide invariant can be defined as:

$$\beta_{ml}=-\frac{\Delta S_{p,ml}\left(\omega\right)}{\Delta S_{g,ml}\left(\omega\right)}; \tag{2}$$

where, $\Delta S_{p,ml}(\omega) = S_{p,m} - S_{p,l}$, $\Delta S_{g,l}(\omega) = S_{g,m} - S_{g,l}$, $S_{p,m}$ and $S_{g,m}$ are the phase slowness (inverse of the phase velocities) and group slowness (inverse of the group velocities) for the *m* mode. β is defined in terms of the slope of that line. Obviously, the acoustic fields accumulated by different modes have different waveguide invariants.

In Fig. 1f all modes with phase velocities larger than 1532 m/s can be connected to a line, where the slope is approximate to -1. The modes with phase velocities less than 1532 m/s cannot be connected to a line. In Fig. 1d all modes can be connected to a line, where the slope is equal to -1.

Regarding the waveguide in Fig. 1c, the phase speed interval of mode *m, i.e.,*1532 m/s $< v_{pm} <$ 1600 m/s, corresponds to SRBR mode, and the waveguide invariant calculated by a pair of modes denoted by *m* and *l* in SRBR is $\beta_{ml} \approx 1$. On the other hand, the modes of waveguide in Fig. 4d are all SRBR modes, which means the aforementioned waveguide invariant for all modes is $\beta_{ml} \approx 1$.

The waveguide invariant in the acoustic field composited by the SRBR modes are likely to be deduced as $\beta \approx 1$, and consistent striation slopes can be observed in the range-frequency spectrum. Nevertheless, this parameter in the acoustic field composed by the non-SRBR modes is not a constant value, thus, a non-consistent striation slope is shown in the range-frequency spectrum.

In the shallow negative thermocline waveguide, the acoustic field striation in the large depth from the shallow source above the thermocline have the consistent striation slopes as the $\beta \approx 1$. The acoustic field striation in the large depth from the depth source below the thermocline have the non-consistent striation slopes as $\beta \approx -3$.

3. FILTERING CHARACTERISTICS OF HORIZONTAL ARRAY BEAMFORMING

The response function of an HLA can be written as[13]

$$\gamma_T\left(\omega,\theta_d,\theta_S,r_c;\mathrm{W}\right)=\sum_m A_m\exp\left(-ik_{rm}r_c\right)\gamma\left(\omega,k_d-k_{mS};\mathrm{W}\right). \tag{3}$$

Where: $[\gamma\left(\omega,k_d-k_{ms};\mathrm{W}\right)=\sum_{n=1}^{J}\exp\left[i\left(k_0\sin\theta_d-k_{rm}\sin\theta_s\right)d_j\right]w_j]$;

- c_0 is the speed of sound at the HLA depth.
- $k_0 = \omega/c_0$ is the wavenumber at the HLA depth (or arbitrary speed in the sound speed profiles).
- θ_d is the observation direction as measured from the broadside of the HLA.
- θ_s is the bearing of the acoustic source as measured from the broadside of the HLA.
- *N* is the number of elements in the HLA.
- $k_d = k_0 sin\theta_d$ is the horizontal wavenumber corresponding to the look direction.
- k_{rm} is the wavenumber of mode *n*.
- $k_{ms} = k_{rm} sin\theta_s$ is the wavenumber of mode *m* along the array due to a source at a bearing θ_s
- $d_j = d(j-1) - d(J-1)/2, j = 1, 2, \ldots, J$.
- J is the number of elements in the HLA. *d* is the sensor space.
- **W** $= [w_1, w_2, \ldots, w_J]^T$ is the array weights column vector.

The magnitude $|\gamma_T(\omega,\theta_d,\theta_s,r_c;\mathbf{W})|$ can be written as in Eq. (4) (see top of the next page).

When array weights column vector **W=1**, the modulation items:

$$\gamma\left(\omega,k_d-k_{mS};W\right)\gamma\left(\omega,k_d-k_{lS};W\right)=\left(\frac{\sin\left(\frac{Nd}{2}\left(k_0\sin\theta_d-k_{rm}\sin\theta_s\right)\right)}{\sin\left(\frac{d}{2}\left(k_0\sin\theta_d-k_{rm}\sin\theta_s\right)\right)}\right)\cdot\left(\frac{\sin\left(\frac{Nd}{2}\left(k_0\sin\theta_d-k_{rl}\sin\theta_s\right)\right)}{\sin\left(\frac{d}{2}\left(k_0\sin\theta_d-k_{rl}\sin\theta_s\right)\right)}\right) \tag{5}$$

Define:

$$x_m = k_0 sin\theta_d - k_{rm} sin\theta_s,$$

$$|\gamma_T(\omega,\theta_d,\theta_s,r_c;W)|^2 = \left|\sum_m A_m \exp(-ik_m r_c)\,\gamma(\omega,k_d-k_{mS};W)\right|^2 = \sum_m A_m^2\,|\gamma(\omega,k_d-k_{mS};W)|^2 + \sum_{m,l;m\neq l}^{M} A_m A_l \cos(\Delta k_{ml} r_c)\,\gamma(\omega,k_d-k_{mS};W)\,\gamma(\omega,k_d-k_{lS};W)\,. \tag{4}$$

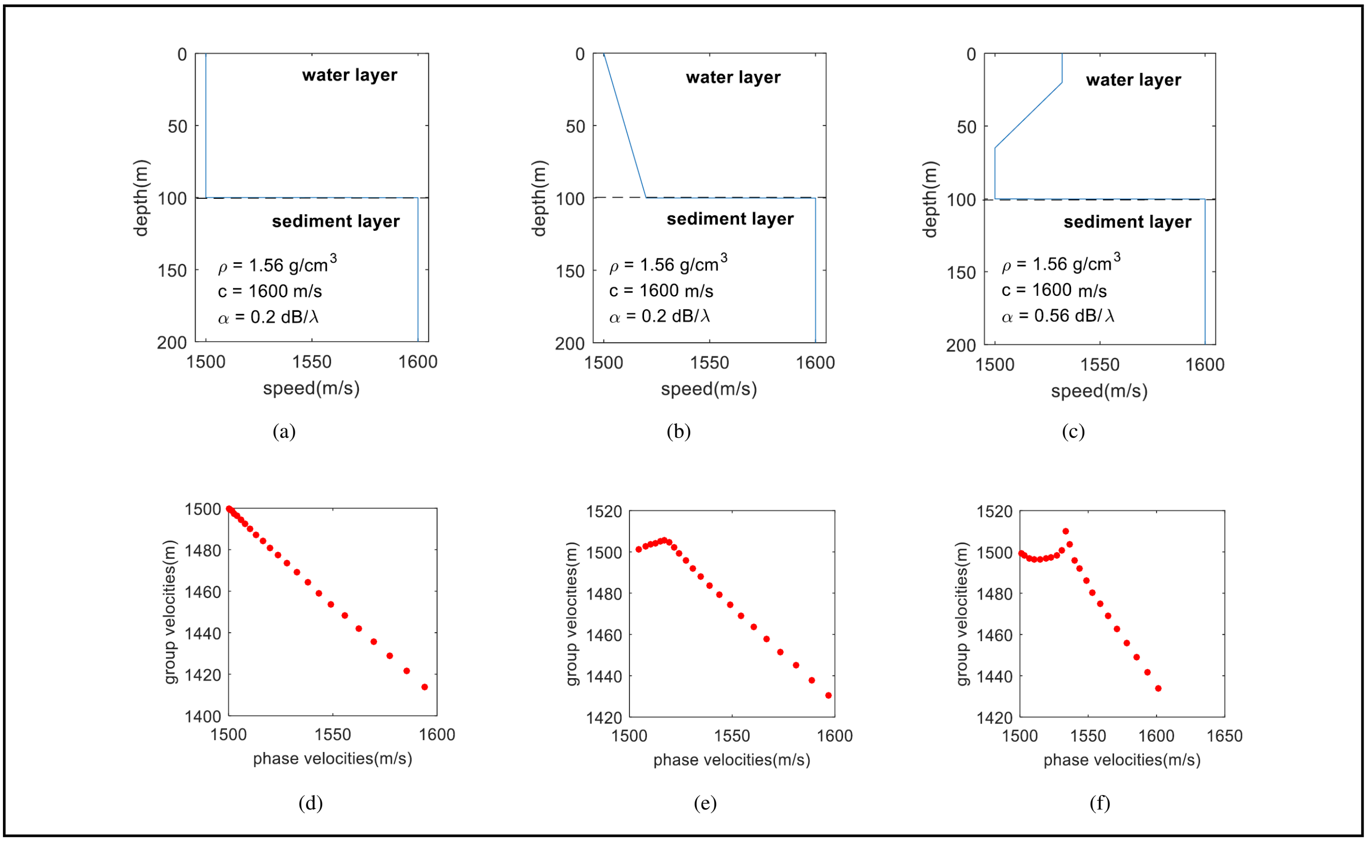

Figure 1. The top row shows the sound speed profiles (pekris waveguide on the left, positive gradient waveguide in the center, negative thermocline waveguide on the right). The plots in the bottom row are group speed versus phase speed at 500 Hz, with each dot corresponding to a mode. The slope of a line connecting points of group slowness (inverse group velocities) versus phase slowness (inverse phase velocities) is the reciprocal of the waveguide invariant.

and the periodic *sinc* function:

$$sinb(x) = sin(xNd/2)/sin(xd/2),$$

as Fig. 2. When $xNd/2 << \pi$, the periodic function $sinb(x)$ is near its maximum value. As $xNd/2$ increases in value, the periodic function $sinb$ decreases in value until $xNd/2 \approx \pi$. Define the half of the main lobe width of $sinb(x)$ as:

$$BW_{1/2} = 2\pi/Nd.$$

When $\theta_d = \theta_s$, we can get $x_m = (k_0 - k_{rm})sin\theta_s$. So if $x > BW_{1/2}$,the value of the $sinb(x_m)$ will be very small, and the m mode contributes little to the beam response function. Therefore, when all $x_m < BW_{1/2}$, the beam output acoustic field is affected by all modes, and its intensity striations are consistent with those of a single hydrophone. However, the longer the array, the smaller the $BW_{1/2}$, and the less mode contributes to the array beam acoustic field. So, it is more obvious with the difference in the output striations of the array and that of the single hydrophone:

Fig. 3a shows that the acoustic field intensity from a short HLA beam output has a distinct intensity level than a bottom receiver, but it has the same striation slope as in Fig. 3b.

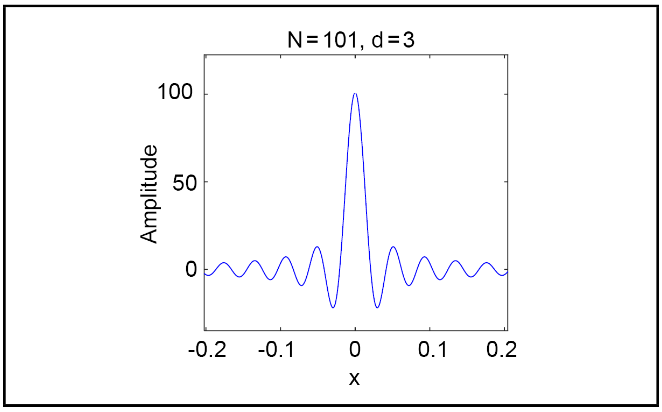

Figure 2. The response of the periodic $sinc$ function $sinb(x_m)$ when the number of elements is 101 in the HLA , where the sensor space $d = 3$ m.

The acoustic field was calculated using Kraken[16] from a range of 3000 m to 5000 m, and a temporal frequency of 200 Hz to 400 Hz. The following simulations are all based on this condition without special denotation.

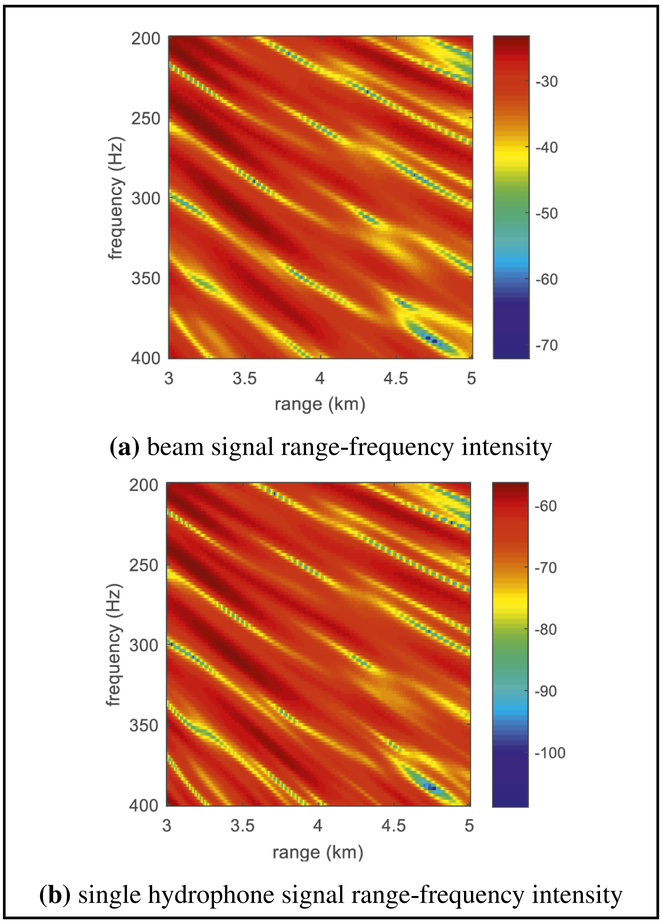

(a) beam signal range-frequency intensity

(b) single hydrophone signal range-frequency intensity

Figure 3. The left plot is the beam intensity as a function of frequency and range for a bottom HLA with 75m length in the fig.1(c) waveguide. The beam is steered at the target, located at the $\theta_d = \theta_s = 90°$.The right plot is the intensity as a function of frequency and range for a single hydrophone of the bottom HLA.

Eqs. 4 and 5 reveal that the interference intensity contributed by the mode m and mode l will be affected by the product of $sinb(x_m)$ and $sinb(x_l)$. When $x_m > BW_{1/2}$, the value of the $sinb(x_m)$ as the product of $sinb(x_m)$ and $sinb(x_l)$ will be very small, despite the value of the x_l. So the interference pattern (striations) of the response function with the uniform weights will be different from the interference pattern present in the single-hydrophone acoustic intensity. The main lobe width of $sinb(x)$ is $4\pi/Nd$, this means that the main lobe width is inversely proportional to the length of the HLA. So combined with the beam response characteristics and the modulation in the Eq. (5), when the length of the HLA increased, the fewer modes contribute to the beam acoustic field. The array response has the mode selection characteristics.

4. CLASSIFICATION METHODS OF SURFACE AND UNDERWATER TARGETS

The purpose of the paper is to discriminate the depth of the underwater acoustic target above or below the thermocline in the typical negative thermocline shallow water environment, which basically corresponds to the working depth of the actual surface and the target of underwater ships and boats. Based on the previous analyses, the target signals received by the long HLA are processed by mean weighted beam processing and frequency adaptive weighted beam processing respectively. The range-frequency spectrum under different processing conditions are obtained. The target depth can be distinguished by analyzing the striation difference of two interference structure patterns. The specific implementation steps are as follows:

- **Step 1**. The target radiated noise range-frequency spectrum (P1) is obtained through the uniformly weighted beamforming in a long horizontal line array by a single hydrophone or short subarrays.

- **Step 2.** According to the FAOW array beam processing method, the array beamforming output of the target radiated noise is obtained. The beam output only contains the acoustic field generated by the accumulation of SRBR modes, and the range-frequency spectrum (P2) under the same parameters in step 1 is obtained.

- **Step 3**. The striation angles ϕ_1 and ϕ_2 of the spectrum P1 and P2 respectively are estimated by the Radon transform.

- **Step 4**. The striation angle difference $\Delta\phi = |\phi_1 - \phi_2|$ is calculated as an identification threshold. When $\Delta\phi < 10°$, the two interference striations are similar to each other, and the target is identified as the surface target. By contrast, when $\Delta\phi > 10°$, the two interference striations are different, and the target is viewed as the underwater target.

5. DISCUSSION

The sound velocity profile of the typical shallow water negative thermocline is shown in Fig. 1c. In the seafloor half-space environment, the sound velocity is 1600 m/s, the density is 1.56 g/cm^3, and the attenuation coefficient is 0.2 dB/λ. The receiving long HLA is fixed at the sea bottom of the depth of 100 m. The number of elements is 201 and the sensor space is 1.5 meters. It is assumed that the depths of the two acoustic source targets are 10 m and 75 m respectively correspond to the surface and underwater targets. Both of them remain in the direction of the end fire of the array, and the relative distance of the array varies from 3000 m to 5000 m. The situation is shown in Fig. 5.

According to the FAOW array beam processing method based on the HLA with 201 elements, the acoustic field modes in the environment as Fig. 5 are filtered. Figs. 6 and 7 show the results of array beam processing with acoustic source depths of 10 m and 75 m, respectively. In the two figures, the left subfigures are the LOFAR spectrum of the signal received by a single hydrophone; the middle subfigures are the FAOW array filtering result of the wavenumber interval $\omega/1532 \sim \omega/1500$; the right subfigures are the result of the wavenumber interval $\omega/1600 \sim \omega/1532$. The results show that the mode separation of HLA beam is realized by FAOW array filtering, and the LOFAR spectrum from different modes are significantly different.

The striations in Fig. 6a are similar to those in Fig. 6c, while the striations in Fig. 7a and Fig. 7c are significantly different. This is because in the typical negative thermocline environment in shallow water, the interference structure of the acoustic intensity radiated by the acoustic source above the thermo-

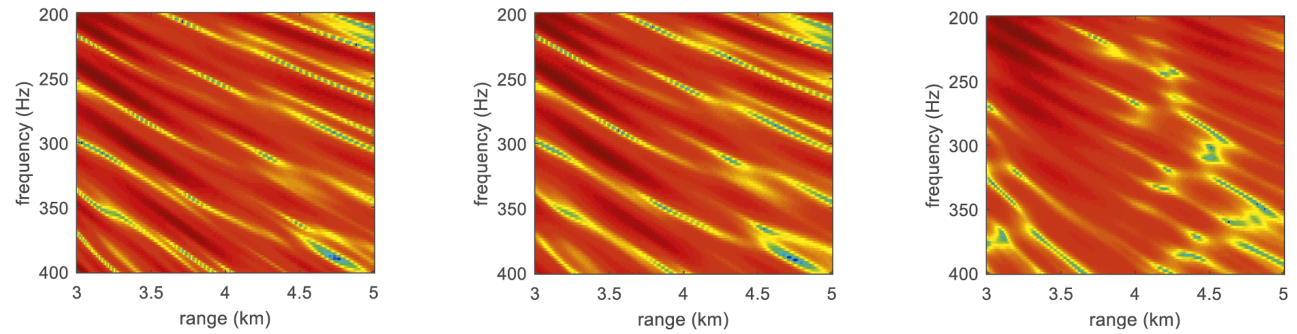

(a) The single hydrophone (b) 75 m HLA response (c) 300 m HLA response

Figure 4. Plots of acoustic intensity as a function of range and frequency with single hydrophone, 75 meters HLA response with uniform weights and 300 meters HLA response with uniform weights. These are from the SSP used for Fig. 1c.

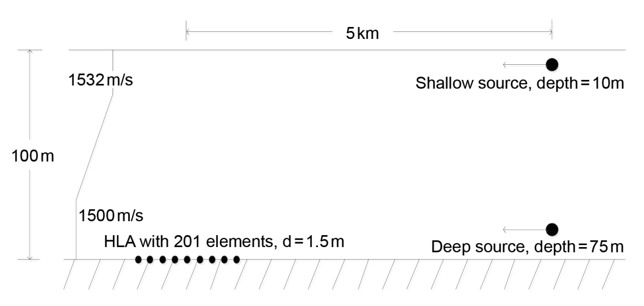

Figure 5. The mutual situation of array and target in the process of numerical erification.

cline is determined by the SRBR modes, while the interference structure in the range-frequency spectrum of the acoustic source under the thermocline is mainly determined by the NSRBR modes.

Figs. 8 and 9 show the processing results of fixed long horizontal line array located at 100 m when the acoustic source depths are 10 m and 75 m, respectively. Among the two figures, the subfigures (a) are the range-frequency spectrum obtained by selecting a subarray with 51 hydrophones for uniform weight conventional beamforming; The subfigures (b) are the striations angle result of the subfigures (a) estimated by Radon transform. and the subfigures (c) are range-frequency spectrum obtained by the HLA with 201 hydrophones using frequency adaptive weighted beamforming (including only SRBR modes). Subfigures (d) are all stripe angle information estimated by Radon transform in subfigures (c).

Furthermore, the striation angle is extracted, and the angle of the interference striations in the range-frequency spectrum generated by the filtered SRBR mode and a single hydrophone output are observed. Considering the actual situation, the signal-to-noise ratio of the target acoustic signal obtained by the single element is low, and the interference striations of the range-frequency spectrum may not be clear. The results of 51-element subarray beamforming are used to replace the single-element results. From the above analysis, the short-array beamforming is basically consistent with the range-frequency spectrum interference structure of the single-element output signal.

According to the striation angle estimation results for the 10m-acoustic source, the output range-frequency spectrum interference striations angle of the uniformly weighted beam of the subarray is $\phi_1 = 74.1°$, and the interference striations angle of the whole array frequency adaptive weighted beam output is $\phi_2 = 69.2°$. The angle difference is $\Delta\phi = 4.9° < 10°$, which can be considered a shallow source target. For the 75 m-acoustic source, the range-frequency spectrum interference striations angle of the subarray uniform weighted beam output is $\phi_1 = 29.4°$, and the whole array frequency adaptive weighted beam output range-frequency spectrum interference striations angle is $\phi_2 = 69.2°$. The angle difference $\Delta\phi = 39.8° > 10°$, meaning the target is identified as a deep source target.

6. CONCLUSIONS

Based on the normal mode theory, this paper first analyzed the difference of the interference striations of the range-frequency structure of the acoustic field when the acoustic field was composed of different types of modes. Then, the reason why the output acoustic field shows modes filtering characteristics when the long HLA is processed by uniform weight beamforming was studied. Further, according to the characteristic that the underwater acoustic target radiation field above and below the negative thermocline was composed of different types of modes, a depth classification of underwater acoustic targets based on long horizontal line array modes filtering was proposed. Finally, the KRAKEN acoustic field model was used to simulate 10 m and 75 m depths acoustic sources, and the above classification method was verified. In the process of beamforming the target with long HLA, the frequency adaptive weighting processing was used to realize that the output acoustic field of the beam was composed of SRBR modes. For the target above the thermocline, the range-frequency spectrum striations of the long HLA FAOW beam output signal were basically the same as the range-frequency spectrum striations of the single hydrophone output signal. On the other hand, for the target under the thermocline, there was a significant difference in the range-frequency spectrum striations between the long HLA FAOW beam output and the single hydrophone output. By analyzing the difference of the range-frequency spectrum interference structure be-tween the long HLA FAOW beam output signal and the single hydrophone (or short subarray uniformly weighted beam) output signal, the surface and underwater characteristics of the target were judged according to the difference. Based on the inherent characteristics of acoustic

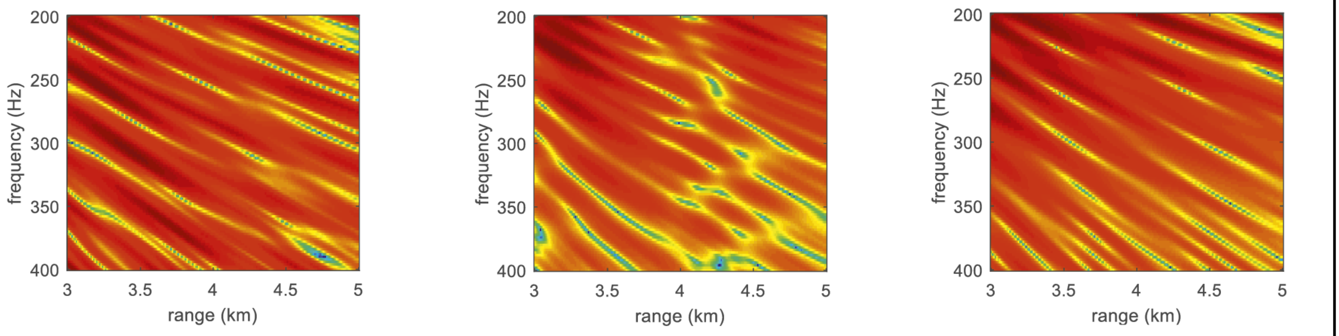

(a) single hydrophone (b) NSRBR modes (c) SRBR modes

Figure 6. LOFAR spectrum comparison of single hydrophone output and horizontal linear array filter output with the acoustic source depth is 10 m.

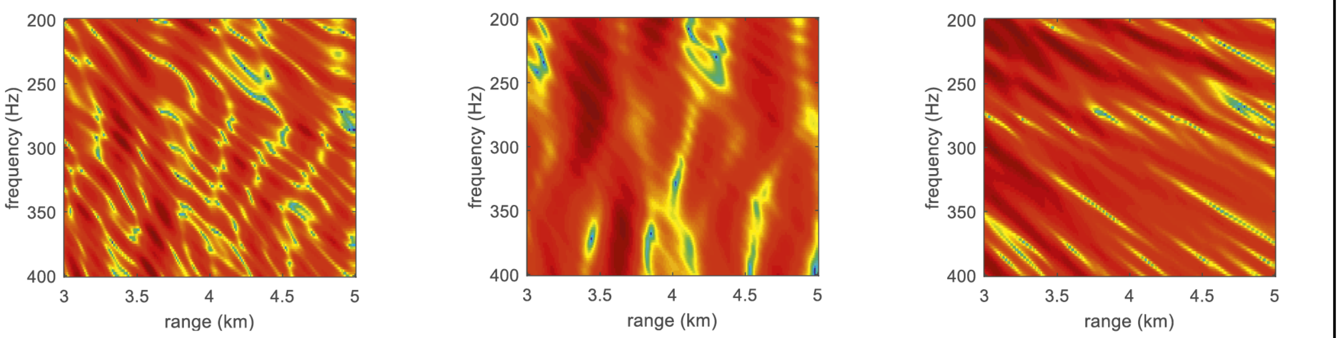

(a) single hydrophone (b) NSRBR modes (c) SRBR modes

Figure 7. LOFAR spectrum comparison of single hydrophone output and horizontal linear array filter output with the acoustic source depth at 75 m.

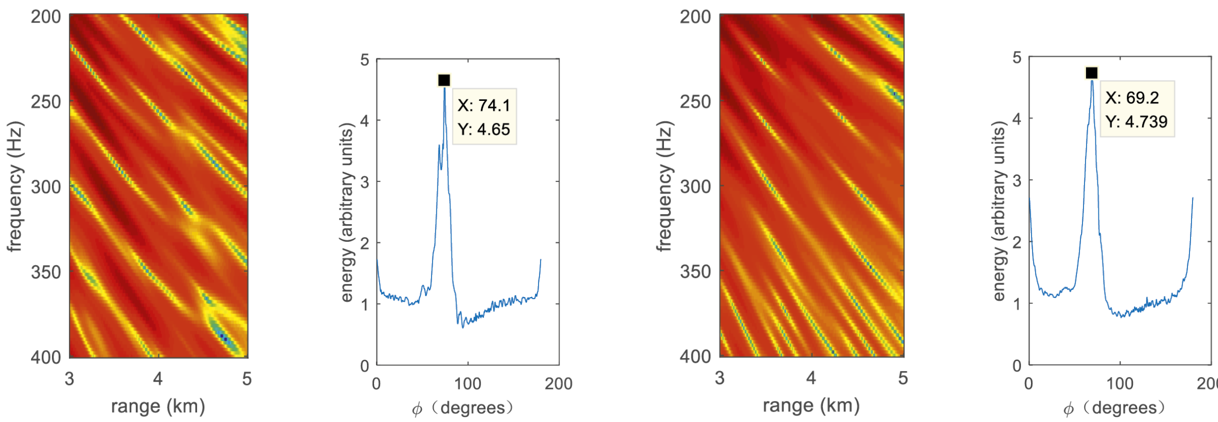

(a) short-array (b) short-array (c) long-array (d) long-array

Figure 8. Processing results and striations estimation of short subarray conventional beam and long array frequency adaptive weighted beam when the acoustic source depth is 10 m.

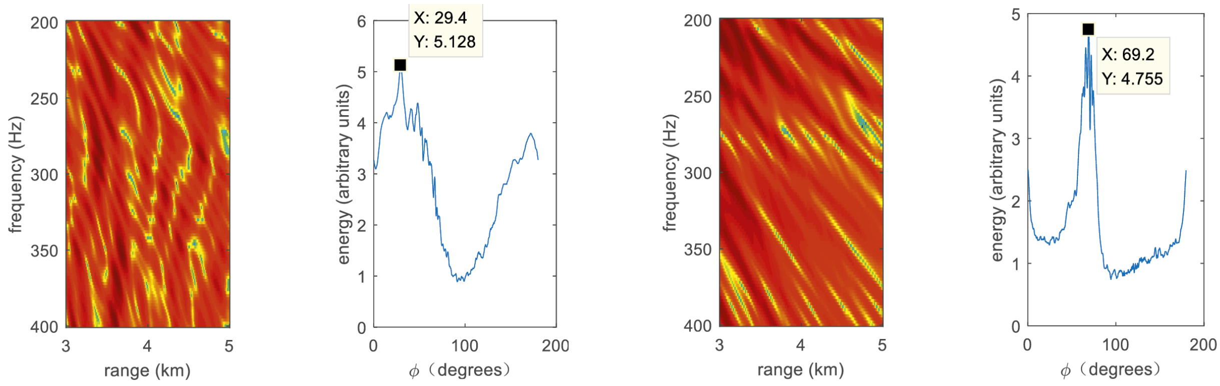

(a) short-array (b) short-array (c) long-array (d) long-array

Figure 9. Processing results and striation estimation of short subarray conventional beam and long array frequency adaptive weighted beam when the acoustic source depth is 75 m.

propagation, this method realized the discrimination of target depth type, the principle is simple, and it is easy to realize, so it has important engineering application value.

REFERENCES

1 Worthmann, B.M., Song, H.C. and Dowling, D.R. High frequency source localization in a shallow ocean sound channel frequency difference matched field processing. *J. Acoust. Soc. Am.*, **138**(6), 3548–3562, (2015). https://dx.doi.org/10.1121/1.4936856

2 Luo, X.Y., Han, Q.B., and Zhou, D.F. Simulation of depth resolution for MFP passive detection. *Applied Mechanics and Materials*. **742**, 136–139, (2015). https://dx.doi.org/10.4028/www.scientific.net/AMM.742.136

3 Turgut, A., Orr, M. and Rouseff, D. Broadband source localization using horizontal-beam acoustic intensity striations. *J. Acoust. Soc. Am.*, **127**(1), 73–83, (2010). https://dx.doi.org/10.1121/1.3257211

4 Yang, K.D., Xu, L.Y., Yang, Q.L. and Duan, R. Striation-based source depth estimation with a vertical line array in the deep ocean. *J. Acoust. Soc. Am.* **143**(1), 8–12, (2018). https://dx.doi.org/10.1121/1.5020267

5 Zhao, A.B., Song, X.J., Hui, J., Zhou, B. and Chen,Y. Research on source depth classification using multiple vector hydrophones. Proceedings of the Oceans 2014 IEEE, Taipei, Taiwan,(2014). https://dx.doi.org/10.1109/OCEANS-TAIPEI.2014.6964438

6 Williams, D. On adaptive underwater object detection. In proceedings of IEEE/RSJ International Conference on Intelligent Robots and Systems. 4741–4748, (2011). https://dx.doi.org/10.1109/IROS.2011.6094621

7 Li, Q.H., Wang, J.L. and Wei, W. An application of expert system in recognition of radiated noise of underwater target. Institute of Acoustics, Chinese Academy of Sciences, Beijing, China, 404–408, (1989). https://dx.doi.org/10.1109/OCEANS.1995.526801

8 Huang, X.Y. ,Zhu, X.B., Xu, K.L. and Wu, J.H. Periodic Signal Detection in Ship Radiated Noise, Advanced Materials Research. **1049**, 1049–1050, (2014). https://dx.doi.org/10.4028/www.scientific.net/AMR.1049-1050.1577

9 Lee, S. Deep learning of submerged body images from 2D sonar sensor based on convolutional neural network, In Proceedings of the 2017 IEEE Underwater Technology(UT), (2017). https://dx.doi.org/10.1109/UT.2017.7890309

10 Medina, E., Petraglia, M.R., and Gomes, J.G.R.C. Comparison of CNN and MLP classifiers for algae detection in underwater pipelines. In Proceedings of the 2017 Seventh International Conference on Image Processing Theory, Tools and Applications(IPTA), (2017). https://dx.doi.org/10.1109/IPTA.2017.8310098

11 Jensen, F.B., Kuperman, W.A., Michael, B.P. and Schmidt, H. *Computational Ocean Acoustics*. Springer Science & Business Media, Berlin, (2011). https://dx.doi.org/10.1007/978-1-4419-8678-8

12 Xu, G.J., Zhao, J.X., Da, L.L. and Han, M. A frequency adaptive optimal array weighted method of interference striations. *Acta Acustica (in Chinese)*, **42**(3), 257–266, (2017) . https://www.researchgate.net/publication/317770844

13 Yang, T.C. Beam intensity striations and applications. *J. Acoust. Soc. Am.*, **113**(3), 1342–1352, (2003). https://dx.doi.org/10.1121/1.1534604

14 Kevin, L. Cockrell and Henrik Schmidt. A modal Wentzel-Kramers-Brillouin approach to calculating the waveguide invariant for non-ideal waveguides. *J. Acoust. Soc. Am.*,**130**(1), 72–83, (2011). https://dx.doi.org/10.1121/1.3592236

15 D'Spain, G.L. and Kuperman, W. A. Application of waveguide invariants to analysis of spectrograms from shallow water environments that vary in range and azimuth. *J. Acoust. Soc. Am.*,**106**(5), 2454–2468, (1999). https://dx.doi.org/10.1121/1.428124

16 Michael, B.P. The kraken normal mode program http://oalib.hlsresearch.com/AcousticsToolbox/. (2020).